Critical Current-Constrained Continuous Nonsingular Terminal Sliding Mode Control for PMSM Based on Control Barrier Function

Bin Dai, Zuo Wang, *Member, IEEE*, Jianfeng Zhao, and Shihua Li, *Fellow, IEEE*

***Abstract*—In this article, the speed regulation control problem for permanent magnet synchronous motor (PMSM) under the single-loop control structure is investigated. Specifically, certain issues, such as the risks of over-current and multisource disturbances, can increase the likelihood of damage to the system circuitry and lead to unsatisfactory speed regulation performance. To tackle these issues, a current-constrained continuous nonsingular terminal sliding mode control (CNTSMC) approach via the control barrier function (CBF) technology is proposed. First, a nonlinear finite-time extended state observer is constructed to estimate the unmatched disturbances in PMSM systems. Subsequently, a new composite CBF-based CNTSMC method incorporating the disturbance estimation is designed, such that the undesirable influence of multisource disturbances on the control performance can be effectively attenuated, while guaranteeing strict current constraints. Finally, the stability analysis of the closed-loop control system is presented. Comparative experimental results demonstrate that the proposed method achieves better speed regulation and critical current constraint performance even in the presence of unmatched disturbances.**

***Index Terms*—Continuous nonsingular terminal sliding mode control (CNTSMC), control barrier function (CBF), current constraint, permanent magnet synchronous motor (PMSM), single-loop control structure, unmatched disturbance.**

I. Introduction

DUE to the inherent attributes of high efficiency, exceptional power density, and remarkable torque-to-inertia ratio, permanent magnet synchronous motors (PMSMs) have been shown widespread applications in various industrial systems, including computer numerical control machines, wind turbine systems and electric vehicles [1], [2], [3]. The high precision and fast dynamic response are emerging as the most important performance indicators in these applications [4]. For achieving these two goals, the cascade control structure is adopted, which involves designing controllers for the speed loop and the q-axis current loop separately [5].

Although this control structure is simple to implement, it can easily lead to difficulties in tuning parameters in practical applications, owing to the fact that the actual control input q-axis voltage and the speed control loop are not in the same channel [6]. Based on this, a novel control structure that combines the speed loop and current loop into a single loop has received widespread attention [7], [8], [9], [10]. Compared to traditional cascade control structures, the single-loop control structure not only has the advantage of more direct control action but also has greater control bandwidth and more superior speed dynamic performance [9], [10]. Despite its merits, it is noteworthy that a saturation function is employed for the reference value of the speed loop under the traditional cascade control structure to guarantee overcurrent protection for PMSM systems [11]. However, within the framework of the single-loop control structure, the q-axis current becomes a system state and cannot be constrained by the same way. Consequently, excessive current poses a significant threat to the circuit safety of PMSMs [12]. Therefore, the design of current constraint must be carefully considered.

Nowadays, various elegant nonlinear control approaches have been investigated for the above issue. One effective solution is the barrier Lyapunov function-based adaptive backstepping control design, which offers theoretical insights in [13] and [14]. However, a key limitation lies in the fact that the virtual control variable is confined within a recursive step, rather than focusing on the q-axis current. Another promising approach is model predictive control, which leverages comprehensive model information to anticipate the future output of the system. The control input is obtained by solving a finite horizon optimization problem with constraints [15]. Unfortunately, the control method may pose challenges in real-time applications due to the conflicting requirements of fast responses and the heavy computational burden imposed by the online optimization [16]. Furthermore, a novel state-constrained controller which combines proportional–differential feedback controller with a penalty term was studied in [17], [18]. As the q-axis current approaches its

Received 3 December 2024; revised 2 March 2025 and 22 April 2025; accepted 30 May 2025. Date of publication 4 June 2025; date of current version 5 August 2025. This work was supported in part by the National Natural Science Foundation of China under Grant 62103102 and Grant 62173221, in part by the Jiangsu Funding Program for Excellent Postdoctoral Talent under Grant 2024ZB055, and in part by the China Postdoctoral Science Foundation under Grant 2024M750423. Recommended for publication by Associate Editor A. M. Bazzi. *(Corresponding author: Zuo Wang.)*

Bin Dai and Jianfeng Zhao are with the College of Information Science and Technology & Artificial Intelligence, Nanjing Forestry University, Nanjing 210037, China (e-mail: b.dai@njfu.edu.cn; zjf211@njfu.edu.cn).

Zuo Wang and Shihua Li are with the School of Automation, Southeast University, Nanjing 210096, China, and also with the Key Laboratory of Measurement and Control of CSE, Ministry of Education, Nanjing 210096, China (e-mail: z.wang@seu.edu.cn; lsh@seu.edu.cn).

Color versions of one or more figures in this article are available at https://doi.org/10.1109/TPEL.2025.3576340.

Digital Object Identifier 10.1109/TPEL.2025.3576340

constraint value, the gain of the penalty term increases, thereby imposing a strict constraint on the current state and ensuring overcurrent protection.

In recent years, the concept of safety control has received attention from many scholars [19], [20]. The core technology for establishing safety constraints is the control barrier function (CBF), which restricts certain state-related control input constraints to guarantee the control invariance of the set [20]. This property ensures that the trajectories of system states stay inside the safe region forever if they start inside this set [21]. However, CBF can only establish safety constraints, but cannot guarantee the stability of the closed-loop control system [21]. A decent approach is to combine the design of the state-stabilizing controller [22].

As is known to all, PMSM is a nonlinear system with multisource disturbances, such as cogging torque, magnetic flux harmonic, parameter perturbation, unknown load torque, and so on [23], [24]. Under the noncascade control framework, the properties of these disturbances are transformed into unmatches that cannot be immediately compensated since they are not in the same channel with control input. This increases the difficulty of controller designs and results in unsatisfactory speed regulation performances [25]. To eliminate the influence of these unmatched disturbances, numerous advanced nonlinear control methods have been proposed. Among them, sliding mode control (SMC) stands out as a nonlinear control approach that exhibits significant robustness in the face of disturbances and uncertainties, which can not only stabilize the PMSM speed regulation systems but also exhibit strong disturbance rejection capabilities [26], [27]. Alternatively, the presence of disturbances often leads to a chattering issue in SMC, stemming from the application of a discontinuous control law with an overestimated switching gain [26], [27]. To address this issue and completely eliminate the chattering phenomenon, an effective solution is to employ a continuous control law instead of the discontinuous one [27], [28]. This approach promises smoother speed tracking ability while maintaining the robust disturbance rejection capabilities inherent in SMC.

Motivated by the above researches, in this article, we focus on improving the speed regulation performance of the PMSM systems under the single-loop control structure with unmatched disturbances, while ensuring the overcurrent protection. First, a finite-time extended state observer (FTESO) is developed to estimate the unmatched disturbances in the PMSM systems. Then, to enhance both the dynamic performance and robustness of the control strategy, a composite continuous nonsingular terminal SMC (CNTSMC) method that incorporates disturbance estimation is proposed. Finally, current constraints are guaranteed via constructing the CBF. The proposed control design is framed as a quadratic program, ensuring that the current trajectories remain confined within the safe set while consistently and effectively mitigating the adverse effects of multisource disturbances on control performance. The presentation outlines the stability evaluation of the closed-loop control system, with the practical effectiveness of the proposed control method being validated through rigorous experimental tests. The main contributions of this article are listed as follows:

1) The authors in [17] and [18] proposed a practical and easy-to-implement current-constrained control method via a well-designed nonlinear penalty term, while they cannot work effectively when the equivalent current value exceeds the limit value. In contrast, the proposed controller guarantees critical current constraints by employing the CBF technique, which can efficiently and promptly suppress the current back within the limit value.
2) The proposed composite CNTSMC control scheme, which incorporates disturbance estimation from FTESO, not only ensures finite-time convergence of closed-loop PMSM systems in the presence of unmatched disturbances but also implements a continuous control law that effectively eliminates the inherent chattering problem in conventional SMC control schemes.
3) The proposed control method can easily be applied to various operating conditions of PMSMs, such as maximum torque per ampere control mode, flux-weakening control mode, and loss minimization control mode. Furthermore, its compact control architecture and comprehensive theoretical validation enable straightforward implementation across numerous motion control systems, significantly expanding its potential applications.

II. Mathematical Model and Problem Analysis

The ideal mathematical model of surface-mounted PMSM in the rotating dq coordinate system is expressed as

$$\begin{cases} \dot{i}_d = \frac{1}{L_s}\left(-R_s i_d + \omega_e L_s i_q + u_d\right) \\ \dot{i}_q = \frac{1}{L_s}\left(-R_s i_q - \omega_e L_s i_d - \omega_e \psi_m + u_q\right) \\ \dot{\omega} = \frac{1}{J}(T_e - B\omega - T_L) \end{cases} \tag{1}$$

where ω represents the mechanical angular velocity, and ω_e stands for the electrical angular velocity, which is related to ω by $\omega_e = n_p\omega$. The stator resistance is denoted by R_s, the number of pole pairs n_p, and the permanent-magnet flux linkage is ψ_m. $i_{d,q}$ and $u_{d,q}$ are dq-axis currents and voltages. In addition, L_s represents the tator inductance, B is the viscous frictional coefficient, J stands for the inertia, T_L is the load torque, T_e represents the electromagnetic torque, and $T_e = 1.5n_p\psi_m i_q$.

The objective is to achieve a high-precision speed tracking control under the single loop structure while considerably realizing current constraint in face of multisource disturbances. Here, the d-axis current loop still uses a PI controller. The reference value of the d-axis current i_d^* depends on the selected operating mode of the surface-mounted PMSM. For instance, when operating in maximum torque per ampere control mode, $i_d^* = 0$ is adopted [29]. When operating in flux-weakening control mode or loss minimization control mode, i_d^* is calculated based on the corresponding model [30]. Define the speed tracking error as $\sigma_1 = \omega_r - \omega$, one obtains

$$\dot{\sigma}_1 = -\frac{K_t}{J} i_q + \frac{B}{J}\omega + d \tag{2}$$

where ω_r is the speed reference signal and $K_t = 1.5n_p\psi_m$. d represents the lumped disturbances in PMSM systems. A modest assumption is given as follows.

Assumption 1: The derivative of the disturbance d is bounded, where $\delta = |\dot{d}(t)|$.

Remark 1: Note that multisource fast and slowly time-varying disturbances widely exist in PMSM, including cogging torque, magnetic flux harmonics, parameter uncertainties, and unknown load torque, etc. [3], [6], [8], [15]. Thus, Assumption 1 aligns well with the practical PMSM applications, as several prior studies have also made similar assumptions regarding d, such as [3], [11], [15], and [18], etc.

III. Controller Design

This section presents the design procedure of the proposed current-constrained control law for the PMSM system.

A. FTESO Design

To achieve better dynamic performance and obtain disturbance information in PMSMs (2), according to [31], the FTESO is designed as follows. For the sake of simplification, denote $\lfloor x \rceil^{\iota} = |x|^{\iota}\text{sign}(x)$, one obtains

$$\begin{cases} \dot{z}_1 = -\frac{K_t}{J} i_q + \frac{B}{J}\omega + z_2 + K_1 f_1(e_1) \\ \dot{z}_2 = K_2 f_2(e_1) \end{cases} \tag{3}$$

where $e_1 = \sigma_1 - z_1$, $f_1(e_1) = \lfloor e_1 \rceil^{r_1} + \lfloor e_1 \rceil^{r_2}$, and $f_2(e_1) = r_1 \lfloor e_1 \rceil^{2r_1-1} + r_2 \lfloor e_1 \rceil^{2r_2-1} + (r_1 + r_2)\lfloor e_1 \rceil^{r_1+r_2-1}$. $r_1 = 1 + \chi$, $r_2 = 1 - \chi$, and $\chi \in (-\frac{1}{2}, 0)$. K_1 and K_2 are the observer gains to be designed. z_1 and z_2 are the estimation of σ_1 and d, respectively.

Remark 2: Compared with the traditional ESO and disturbance observer (DOB) which can only realize the asymptotic convergence of the slow-varying disturbance [8], [18], the proposed FTESO can realize the finite-time convergence of the fast and slowly time-varying disturbances in system (2). K_1 and K_2 play a same role in adjusting the convergence rate of the observer estimation error in both ESO and FTESO.

Remark 3: The larger χ, the faster the convergence of the disturbance estimation error system, but also increases the measurement noise effect in practical applications. Therefore, the selection of χ should be balanced between the convergence rate and performance of the disturbance estimation error.

B. Composite CNTSMC Method Design

To eliminate the chattering influence, a continuous nonsingular terminal sliding mode manifold based on [28], which combines the disturbance estimation by FTESO (3) for PMSM system (2) is designed as

$$s = \sigma_1 + \frac{1}{m}\lfloor \sigma_2 \rceil^n \tag{4}$$

where $\sigma_2 = -\frac{K_t}{J} i_q + \frac{B}{J}\omega + z_2$. $1 < n < 2$ and $m > 0$ are the controller parameters to be designed. Taking the derivative of s, one obtains

$$\begin{aligned} \dot{s} &= \dot{\sigma}_1 + \frac{n}{m}|\sigma_2|^{n-1}\dot{\sigma}_2 \\ &= \dot{\sigma}_1 + \frac{n}{m}|\sigma_2|^{n-1}\left(\epsilon - \frac{B}{J}d + \dot{z}_2 - \frac{K_t}{JL_s}u_q\right) \end{aligned} \tag{5}$$

where $\epsilon = \frac{K_t R_s}{JL_s} i_q + \frac{K_t}{JL_s}\omega_e \psi_m + \frac{K_t B}{J^2} i_q - \frac{B^2}{J^2}\omega$. Combining the disturbance estimation from FTESO (3) with (5), the CNTSMC controller u_s can be deduced as

$$\begin{aligned} u_s = &\frac{JL_s m}{K_t n}\left(\lfloor \sigma_2 \rceil^{2-n} + k_1 s + k_2 \lfloor s \rceil^{\gamma}\right) \\ &+ \frac{JL_s}{K_t}\left(\epsilon - \frac{B}{J} z_2 + \dot{z}_2\right) \end{aligned} \tag{6}$$

where $0 < \gamma < 1$. k_1 and k_2 are the controller parameters to be designed.

C. Current-Constrained Controller Design

The proposed CNTSMC controller u_s can only guarantee the stability of the closed-loop PMSM system, but not the ability on the current constraints. Suppose that the q-axis current i_q should be limited within a constant boundary, i.e., $|i_q| \le c$. In this way, it is equivalent to i_q is constrained between the upper constraint boundary $\overline{h}(i_q)$ and the lower constraint boundary $\underline{h}(i_q)$, which are described as

$$\begin{cases} \overline{h}(i_q) = c - i_q \\ \underline{h}(i_q) = c + i_q. \end{cases} \tag{7}$$

Based on (7), a safe set $\mathcal{C}_{iq}$ is defined as

$$\mathcal{C}_{iq} = \{i_q \in \mathbb{R} : -c \le i_q \le c\}. \tag{8}$$

Lemma 1 [19]: Consider the following nonlinear control-affine system:

$$\dot{x} = f(x) + g(x)u \tag{9}$$

with system state $x \in \mathbb{R}^n$ and control input $u \in \mathbb{R}$. The functions $f(x) : \mathbb{R}^n \to \mathbb{R}^n$ and $g(x) : \mathbb{R}^n \to \mathbb{R}^n$ are locally Lipschitz with respect to its arguments. We call the function $h(x)$ is a CBF on the set $\mathcal{C} = \{x \in \mathbb{R}^n : h(x) \ge 0\}$ for system (9), if there exists a extended class $\mathcal{K}$ function τ make the following condition holds:

$$\sup_{u \in U}\{L_f h(x) + L_g h(x) u + \tau(h(x))\} \ge 0 \tag{10}$$

where $L_f h(x) = \frac{\partial h(x)}{\partial x} f(x)$ and $L_g h(x) = \frac{\partial h(x)}{\partial x} g(x)$ are standard Lie derivatives.

With Lemma 1 in mind, to achieve the current constraints, the CBF for dynamics of i_q in system (1) is defined as follows.

Definition 1: Under the given safe set $\mathcal{C}_{iq}$, if there exists a positive constant τ_1 such that

$$\sup_{u \in \mathbb{U}}\left\{\frac{R_s i_q}{L_s} + \omega_e i_d + \frac{\omega_e \psi_m}{L_s} - \frac{u_q}{L_s}\right\} \ge -\tau_1 \overline{h}(i_q) \tag{11}$$

and

$$\sup_{u \in \mathbb{U}}\left\{-\frac{R_s i_q}{L_s} - \omega_e i_d - \frac{\omega_e \psi_m}{L_s} + \frac{u_q}{L_s}\right\} \ge -\tau_1 \underline{h}(i_q) \tag{12}$$

satisfy, the functions $\overline{h}(i_q)$ and $\underline{h}(i_q)$ are CBFs for the PMSM system, where U is the input constraint set.

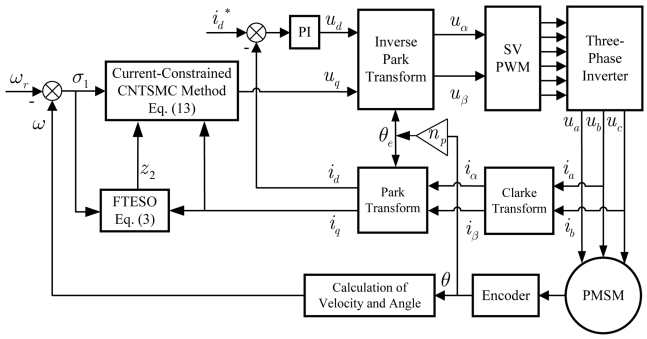

Fig. 1. Schematic diagram of PMSM under the proposed control method.

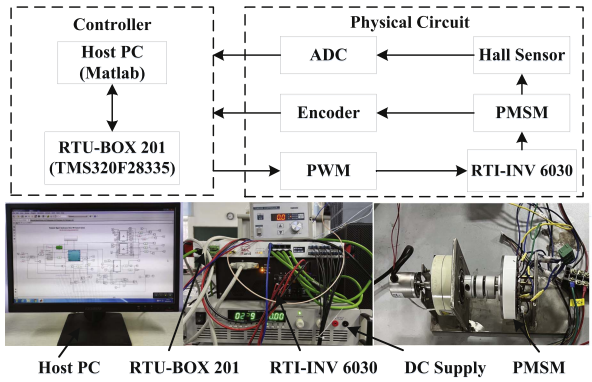

Fig. 2. Experiment system.

Finally, the composite current-constrained CNTSMC method (13) via CBF is proposed and can be transformed into a constrained quadratic programming problem as follows:

$$\begin{aligned} u_q^* = & \underset{u_q\in\Omega}{\operatorname{argmin}} \frac{1}{2}||u_q - u_s||^2 \\ \text{s.t. } & \frac{R_s i_q}{L_s} + \omega_e i_d + \frac{\omega_e \psi_m}{L_s} - \frac{u_q}{L_s} \geq -\tau_1 \overline{h}(i_q) \\ & -\frac{R_s i_q}{L_s} - \omega_e i_d - \frac{\omega_e \psi_m}{L_s} + \frac{u_q}{L_s} \geq -\tau_1 \underline{h}(i_q) \end{aligned} \tag{13}$$

where Ω is the input constraint set.

The control block diagram of the proposed current-constrained CNTSMC method is presented in Fig. 1.

Remark 4: Control design (13) corrects the control input u_s that ensures stability and filters out the control input u_s that violates current constraints. As a result, after being filtered by CBF, u_q^* is the most suitable control input that is closest to u_s, ensuring both stability and satisfaction of current constraints.

Remark 5: The parameter τ_1 is employed to adjust the constraint ability of the current. The smaller τ_1 is, the stronger suppression ability of i_q becomes, and vice versa.

Remark 6: In the MPC design, in order to obtain a high-precision control effect, the control horizon and prediction horizon are selected to be larger, which requires a longer calculation time to execute the algorithm. In contrast, the proposed control method is purely a numerical solution and does not involve matrix operations. Therefore, the computational burden of the proposed control algorithm is significantly lower than that of the MPC methods discussed in [15] and [34].

The stability analysis of the closed-loop PMSM system is given by the following theorem.

Theorem 1: Suppose that Assumption 1 is satisfied for PMSM system (2). If the observer gains and the control parameters are selected properly, both the speed tracking and the disturbance estimation errors can converge to zero, while ensuring the critical current constraints.

Proof: See Appendix.

IV. Experiment Test Results

In this section, we verify the speed regulation performance and current constraint performance of the proposed method by comparison with the three methods in the presence of unmatched disturbances thought experiment tests. The first and second are the designed CNTSMC methods (6) which remove the design of CBF, named CNTSMC-B and CNTSMC-S, respectively. Among these, CNTSMC-S selects conservative control parameters to ensure current constraints during the startup phase. The third method is the DOB-based current constrained (DOB-CC) controller in [18].

TABLE I
Parameters of PMSM

Parameters	Nominal Value
Rated power P_N	225w
Rated voltage U_N	48V
Rated current I_N	4.7A
Rated load T_N	$0.273\text{N}\cdot\text{m}$
Bus voltage U_{dc}	24V
Stator resistance R_s	0.72Ω
Stator inductance L_s	1mH
Number of pole pairs n_p	4
Flux linkage ψ_m	0.014Wb
Rotational inertia J	$7.06\times10^{-4}\text{kg}\cdot\text{m}^2$
frictional coefficient B	$3.5\times10^{-4}\text{N}\cdot\text{m}\cdot\text{s/rad}$

The experiment system, which includes the real-time digital controller RTU-BOX 201, RTI-INV 6030, and a switching power supply, is shown in Fig. 2. The core control chip of the RTU-BOX 201 is the TMS320F28335 (DSP). Utilizing the RTU-BOX 201, the code generated from the control algorithm model in Simulink can be directly downloaded to the DSP. The RTI-INV 6030 incorporates a comprehensive set of components, including a three-phase inverter drive, a three-phase inverter bridge, and acquisition circuits. The PMSM system utilizes a magnetic powder brake as its load. To acquire the motor's position and speed data, an incremental encoder featuring 2048 lines is employed. The experimental configuration is interfaced with a host computer, and the control system operates with a sampling frequency of 10 kHz. Table I details the parameters of the PMSM.

The current constraint value is set as $c = 8$ A, and the reference speed $\omega_r = 1000$ r/min. In the proposed control method, $\tau_1 = 1000$ is set, and the other control parameters of these four control methods can be found in Table II.

TABLE II
PARAMETERS OF FOUR CONTROL METHODS IN THE EXPERIMENTS

Controllers	Parameters	
Proposed	$\alpha = 1.5$, $\gamma = 0.5$	$\beta = 1800$, $k_1 = k_2 = 20$
CNTSMC-B	$K_1 = 400$, $K_2 = 40\,000$	
CNTSMC-S	$\chi = -0.3$	$\beta = 1500$, $k_1 = k_2 = 20$
DOC-CC	$K_p = 30$, $K_d = 0.02$	$p = 600$ (DOB gain)

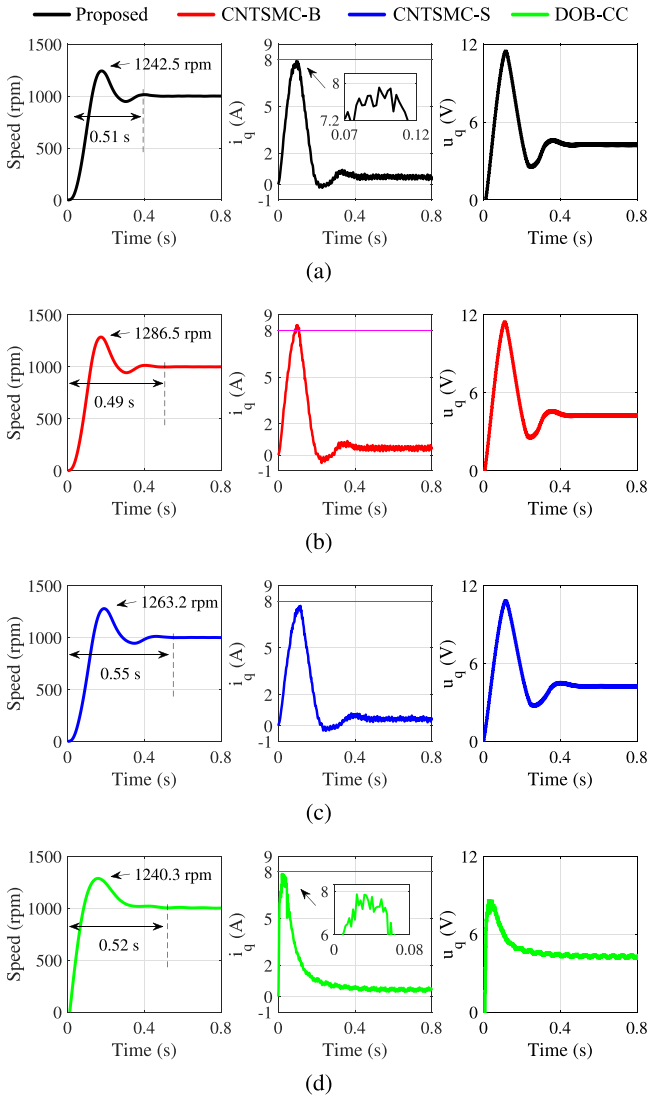

Fig. 3. Response curves of speed ω, q-axis current i_q and q-axis voltage u_q at startup phase. (a) Proposed method. (b) CNTSMC-B. (c) CNTSMC-S. (d) DOB-CC.

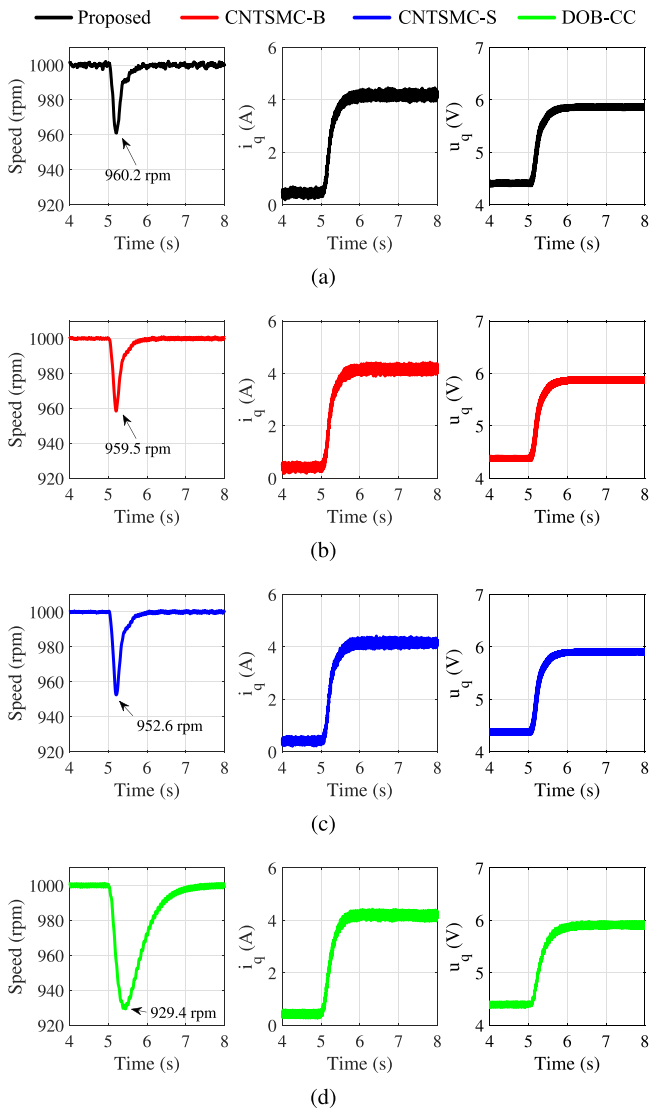

Fig. 4. Response curves of speed ω, q-axis current i_q and q-axis voltage u_q at step load phase with $T_L = 0.3\ \mathrm{N{\cdot}m}$. (a) Proposed method. (b) CNTSMC-B. (c) CNTSMC-S. (d) DOB-CC.

A. Speed Tracking Performance

In this case, the reference value of the d-axis current is set as $i_d^* = 0$ A. the load torque is anticipated to undergo a step change of $0.3\ \mathrm{N{\cdot}m}$ and a sinusoidal variation of $0.2\sin(4\pi t) + 0.2\ \mathrm{N{\cdot}m}$ at $t = 5$ s, respectively. Figs. 3–5 show the response curves of the speed ω, q-axis current i_q and q-axis voltage u_q at startup phase, step load torque phase and sinusoidal load torque phase, respectively. To evaluate the control capabilities of these four controllers more thoroughly, we consider the following performance metrics: For the no-load start-up phase, we compare the overshoot (OS), settling time (ST), and root-mean-square error (RMSE); during the step load torque phase, we use the speed drop (SD), recovery time (RT), and RMSE for comparison; and for the sinusoidal load torque phase, we employ the speed fluctuation (SF) and RMSE as a comparison metric. The results are shown in Table III.

As shown in Fig. 3 and Table III, we can conclude that the startup phase of the controllers exhibits the shortest ST under the CNTSMC-B method and the longest ST under the CNTSMC-S method, when compared to the other two controllers in the group. Both the proposed control method and the DOB-CC control method exhibit similar OS and ST, indicating that the control energy utilized by these two methods is quite comparable. In addition, the two control methods achieve the current constraints. According to Figs. 4 and 5 and Table III, one has

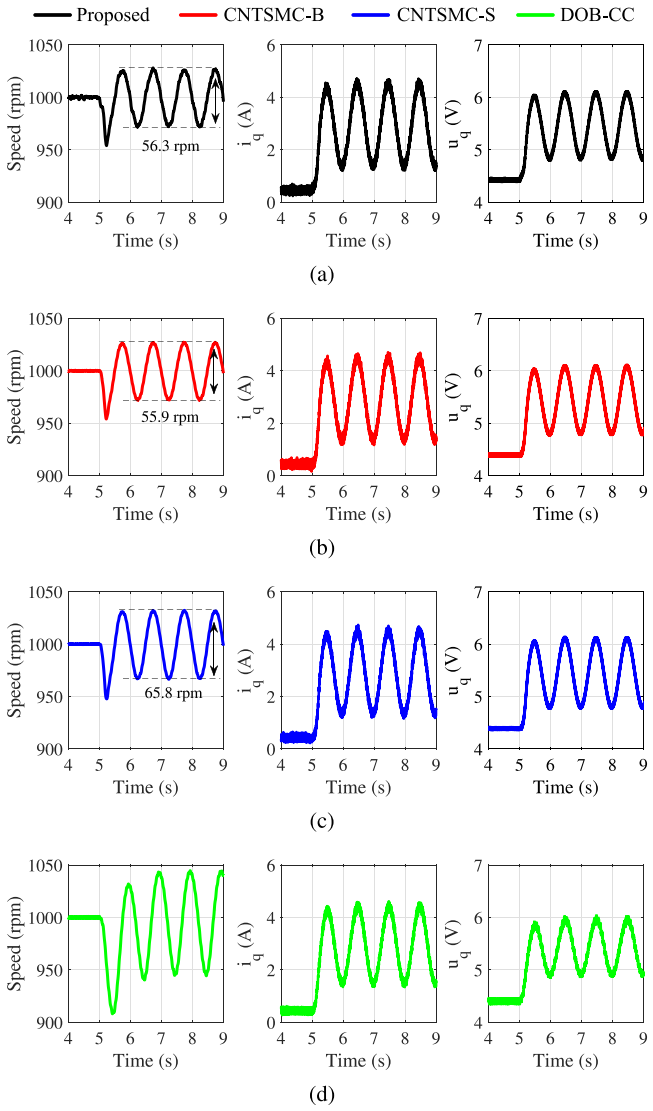

Fig. 5. Response curves of speed ω, q-axis current i_q and q-axis voltage u_q at sinusoidal load phase with $T_L = 0.2\sin(4\pi t) + 0.2$ N·m in the experiments. (a) Proposed method. (b) CNTSMC-B. (c) CNTSMC-S. (d) DOB-CC.

that SDs and SFs under the proposed and CNTSMC-B control methods are similar, and SD and SF under DOB-CC method is most during the different load torques. If conservative control parameters are selected to satisfy the overcurrent protection of the PMSM system, the speed response becomes very poor in the face of different disturbances. The speed responses of DOB-CC under different types of loads are the worst, which fully demonstrates the superior antidisturbance performance of the disturbance estimation-based SMC method.

B. Critical Current Constraint Performance

In this case, the reference value of the d-axis current is set as $i_d^* = 0$ A. The load torque is expected to have a step and sinusoidal changes from 0.6 N·m and $0.3\sin(4\pi t) + 0.32$ N·m at $t = 5$ s, respectively. The response curves of speed ω, q-axis current i_q and q-axis voltage u_q under the four control methods

TABLE III
PERFORMANCE COMPARISONS IN THE CASE I

Test type	Performance	**Proposed**	CNTSMC-B	CNTSMC-S	DOB-CC
Startup	OS [r/min]	**242.1**	286.5	278.2	240.3
	ST [s]	**0.51**	0.49	0.55	0.52
	RMSE [r/min]	**203.2**	205.9	205.2	208.6
Step load	SD [r/min]	**39.8**	40.5	47.4	70.6
	RT [s]	**0.98**	1.07	1.22	2.02
	RMSE [r/min]	**10.5**	9.8	11.4	18.6
Sine load	SF [r/min]	**56.3**	55.9	65.8	102.4
	RMSE [r/min]	**22.5**	21.7	27.3	45.6

are displayed in Figs. 6 and 7, respectively. It can be concluded that due to the added load torque, the current equivalent value exceeds the current constraint of 8 A. Since the CNTSMC-B and CNTSMC-S control methods do not incorporate the CBF design, the current surpasses the constraint value when operating at different load conditions. Moreover, the DOB-CC control method fails to constrain the current when the current equivalent value exceeds the constraint, and furthermore, the speed fluctuates violently. This is attributed to the penalty term $1/(c^2 - i_q^2)$ becoming negative, leading to instability in the entire closed-loop system. Such a scenario must be avoided in practical PMSM applications to prevent potential safety hazards. In contrast, the proposed method demonstrates no significant fluctuations in speed under different load conditions and ensures strict current constraints. This indicates that the proposed method effectively protects against system circuit damage caused by excessive current, ensuring the safety and reliability of the system.

C. Flux-Weakening Control Performance

To better highlight the effectiveness of the proposed control method, we consider the low-load and high speed operation with flux-weakening control. The speed reference signal is set as $\omega_r = 2000$ r/min. At $t = 5$ s, the load torque T_L is anticipated to undergo a step change from 0 to 0.3 N·m, while simultaneously, the reference value of the d-axis current i_d^* experiences a step change from 0 to -3 A. Since the DOB-CC method in [18] is designed under the condition $i_d^* = 0$, only the proposed control method, the CNTSMC-B method, and the CNTSMC-S method are considered in this case. Then, as the reference speed signal increases from 1000 to 2000 r/min, the CNTSMC-S method requires more conservative control parameters to ensure current constraints during the no-load start-up phase. Therefore, in this case, we choose $\beta = 1200$, $k_1 = k_2 = 16$, and keep all other parameters unchanged. In addition, the proposed method and the CNTSMC-B method maintain the same control parameters as in Table II.

The response curves of speed ω, q-axis current i_q, q-axis voltage u_q, d-axis current i_d, and d-axis voltage u_d under the three control methods are displayed in Fig. 8. To further assess the control performances of these three controllers, OS, ST, and RMSE are used for the comparisons at no-load start-up phase. At the step load torque phase, SD, RT, and RMSE are employed for comparisons. The results are shown in Table IV.

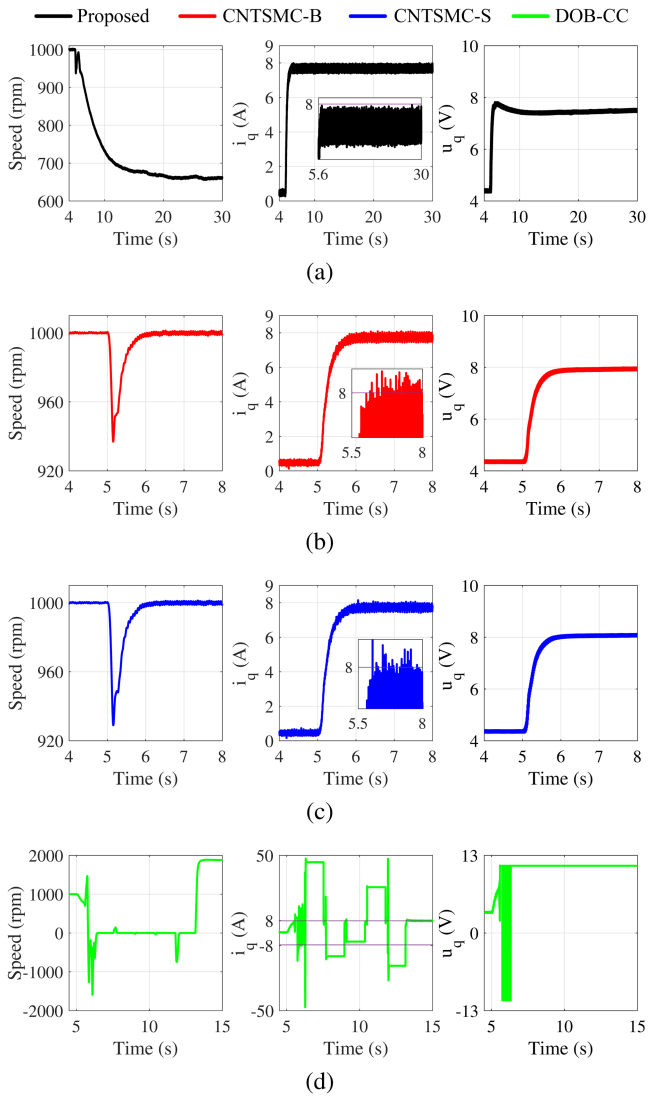

Fig. 6. Response curves of speed ω, q-axis current i_q and q-axis voltage u_q at step load phase with $T_L = 0.6$ N·m. (a) Proposed method. (b) CNTSMC-B. (c) CNTSMC-S. (d) DOB-CC.

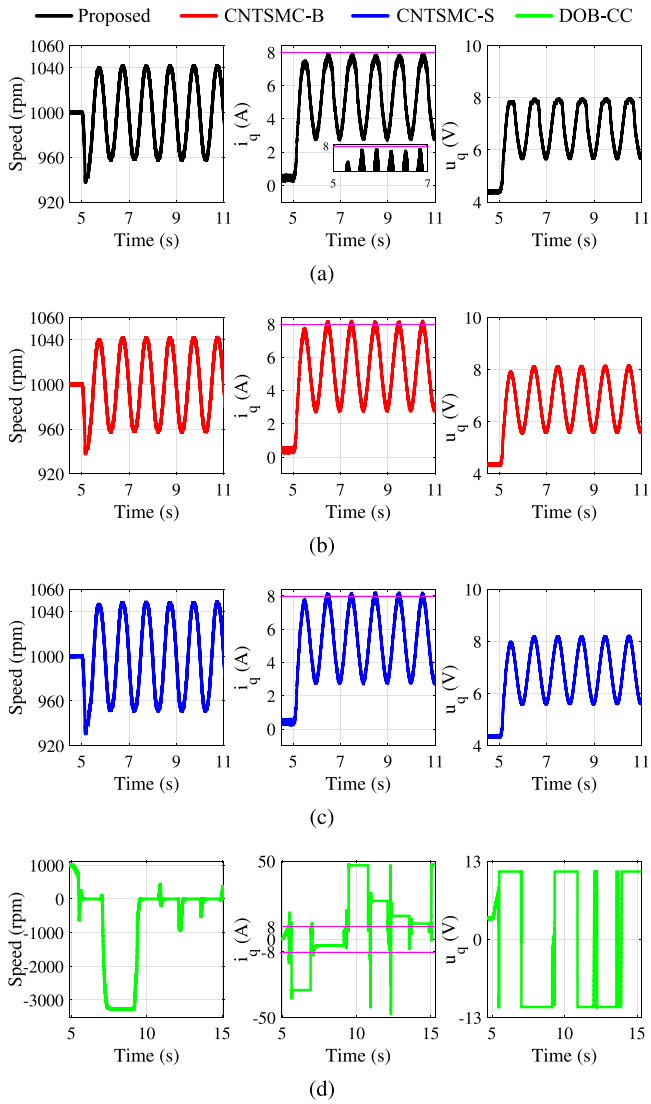

Fig. 7. Response curves of speed ω, q-axis current i_q and q-axis voltage u_q at sinusoidal load phase with $T_L = 0.3\ \sin(4\pi t) + 0.32$ N·m. (a) Proposed method. (b) CNTSMC-B. (c) CNTSMC-S. (d) DOB-CC.

TABLE IV
PERFORMANCE COMPARISONS IN THE CASE III

Test type	Performance	**Proposed**	CNTSMC-B	CNTSMC-S
Start-up	OS [r/min]	**55.3**	51.9	74.6
	ST [s]	**0.64**	0.62	0.78
	RMSE [r/min]	**376.5**	371.1	398.3
Step load	SD [r/min]	**58.5**	58.4	91.2
	RT [s]	**1.36**	1.36	1.59
	RMSE [r/min]	**9.22**	9.23	20.37

Combining Fig. 8 with Table IV, it can be observed that during the startup phase, the CNTSMC-B method, due to its lack of current-limiting mechanism, achieves the smallest OS and shortest ST, exhibiting the fastest dynamic speed response. However, this comes at the cost of a current peak significantly exceeding the 8 A limit. The CNTSMC-S method, while achieving current constraints through conservative parameter selection, exhibits the slowest speed tracking performance due to compromised dynamic response. Unlike the two baseline control approaches, the proposed CBF-based method rigorously enforces current constraints even under control input saturation during speed regulation, as verified by the voltage profiles. Then, both the CNTSMC-B method and the proposed method exhibit constrained control input behavior due to the use of larger control parameters. As the speed rises, the speed tracking error diminishes, the required control effort gradually decreases. Consequently, the control input slowly declines until reaching steady-state operation. In contrast, the CNTSMC-S method employs conservative control parameters, resulting in an unconstrained control input. Nevertheless, regardless of whether u_q is constrained or not, all three methods successfully achieve real-time tracking of the target reference speed. During the loading phase, the proposed method and CNTSMC-B exhibit comparable speed

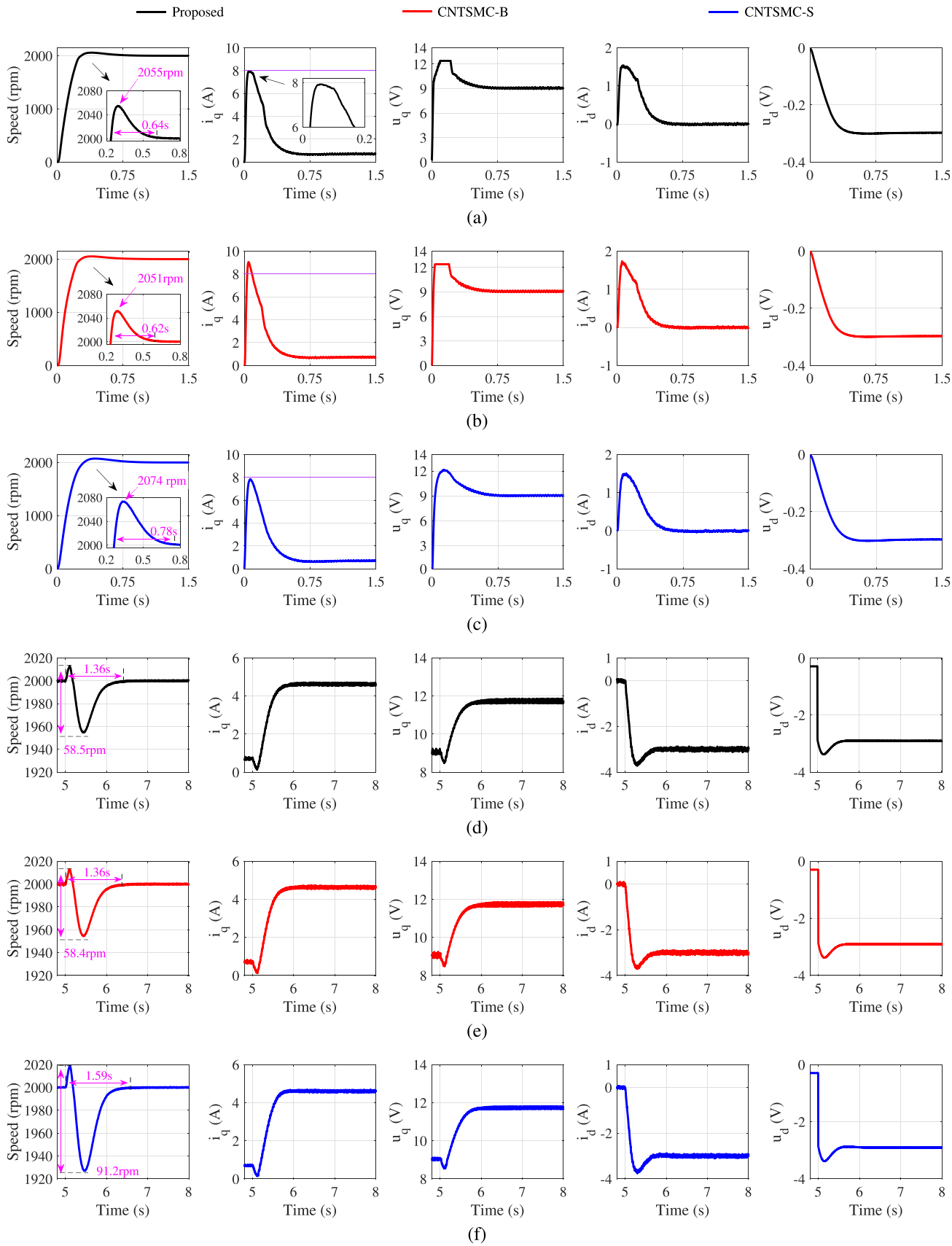

Fig. 8. Response curves of speed ω, q-axis current i_q, q-axis voltage u_q, d-axis current i_d, and d-axis voltage u_d. (a) Start-up phase under the proposed method. (b) Start-up phase under the CNTSMC-B method. (c) Start-up phase under the CNTSMC-S method. (d) Step load phase under the proposed method. (e) Step load phase under the CNTSMC-B method. (f) Step load phase under the CNTSMC-S method.

responses as their equivalent q-axis currents remain well within the constraint limit. In contrast, CNTSMC-S demonstrates larger SD and significantly longer ST, clearly indicating its inferior disturbance rejection capability. In summary, when adopting the flux-weakening control strategy, although the reference value of the d-axis current is set to a negative value to ensure the speed tracking in the high-speed region, the proposed control method can still ensure superior speed tracking performance while achieving strict current constraints.

V. Conclusion

In this article, a novel FTESO-based current-constrained CNTSMC method for PMSM under single-loop control structure has been proposed. This control method not only ensures superior speed tracking performance under the unmatched fast and slowly time-varying disturbances but also achieves overcurrent protection. Notably, the proposed approach can operate effectively in various modes, such as maximum torque per ampere control and flux-weakening control, etc. The experimental results have verified the effectiveness and robustness of the proposed controller.

Appendix

The proof of Theorem 1 is structured into three distinct parts as follows. First, the disturbance estimation error system exhibits finite-time stability is demonstrated. The second is to prove that the speed tracking error under the action of u_s converges to zero in finite time. Finally, we prove that the current constraint is ensured all the time.

A. Step One

Define the disturbance estimation error $e_2 = d - z_2$, with the speed tracking error e_1 and Assumption 1 in mind, the estimation error system is given as

$$\begin{cases} \dot{e}_1 = e_2 - K_1 f_1(e_1) \\ \dot{e}_2 = -K_2 f_2(e_1) + \delta. \end{cases} \tag{14}$$

Let $\varphi = [f_1(e_1), e_2]^T$, it yields

$$\dot{\varphi} = F(e_1)(A\varphi + B\zeta) \tag{15}$$

where $F(e_1) = r_1|e_1|^{r_1-1} + r_2|e_1|^{r_2-1}$, $\zeta = \frac{\delta}{F(e_1)}$, $A = \begin{bmatrix} -K_1 & 1 \\ -K_2 & 0 \end{bmatrix}$, and $B = \begin{bmatrix} 0 \\ 1 \end{bmatrix}$. From (15), one has that matrix A can become the Hurwitz matrix by choosing appropriate observer parameters.

Choose the energy function V_1 as

$$V_1 = \varphi^T Q \varphi. \tag{16}$$

Through this positive-definite function, we have $\lambda_{\min}\{Q\}||\varphi||^2 \le \varphi^T Q \varphi \le \lambda_{\max}\{Q\}||\varphi||^2$ with $\lambda_{\min}$ and $\lambda_{\max}$ represent the minimum and maximum eigenvalues of matrix Q. Due to $\varphi = [f_1(e_1), e_2]^T$ and $0 < \frac{1-r_1}{r_1} < 1$, it yield

$$(|e_1|^{r_1})^{\frac{1-r_1}{r_1}} \le \left(\frac{V_1^{\frac{1}{2}}}{\lambda_{\min}^{\frac{1}{2}}\{Q\}} \right)^{\frac{1-r_1}{r_1}}. \tag{17}$$

Taking the derivative of V_1, one obtains

$$\begin{aligned} \dot{V}_1 &= F(e_1) \begin{bmatrix} \varphi \\ \zeta \end{bmatrix}^T \begin{bmatrix} A^T Q + QA & QB \\ B^T Q & 0 \end{bmatrix} \begin{bmatrix} \varphi \\ \zeta \end{bmatrix} \\ &\le F(e_1) \left\{ \begin{bmatrix} \varphi \\ \zeta \end{bmatrix}^T \begin{bmatrix} A^T Q + QA & QB \\ B^T Q & 0 \end{bmatrix} \begin{bmatrix} \varphi \\ \zeta \end{bmatrix} + \Delta \right\} \end{aligned} \tag{18}$$

where $\Delta = \begin{bmatrix} \varphi \\ \zeta \end{bmatrix}^T \begin{bmatrix} R & S^T \\ S & -\nu I \end{bmatrix} \begin{bmatrix} \varphi \\ \zeta \end{bmatrix}$ and $\nu \ge 0$. According to the analysis in [31], there must exist matrices S and R, and a positive constant μ such that $\Delta \ge 0$ and $\begin{bmatrix} A^T Q + QA + \mu Q + R & QB + S^T \\ B^T Q + S & -\nu I \end{bmatrix} \le 0$. Combining the above analysis with (17), one has

$$\begin{aligned} \dot{V}_1 &\le F(e_1) \begin{bmatrix} \varphi \\ \zeta \end{bmatrix}^T \begin{bmatrix} -\mu Q & 0 \\ 0 & 0 \end{bmatrix} \begin{bmatrix} \varphi \\ \zeta \end{bmatrix} \\ &\le -r_1 |e_1|^{r_1 - 1} \mu V_1 \\ &\le -r_1 \lambda_{\min}^{\frac{1-r_1}{2r_1}} Q \mu V_1^{\frac{3r_1-1}{2r_1}}. \end{aligned} \tag{19}$$

From (19), it can obtain that the estimation error system (14) is finite-time stable.

B. Step Two

According to the analysis in Step 1, there exists time constant t_f such that the estimation errors converge to zero for $t \ge t_f$. When $t < t_f$, it is required to provide proof that the system states will not escape to infinity. Choose the energy function V_2 as

$$V_2 = \frac{1}{2}(s^2 + \sigma_1^2 + \sigma_2^2). \tag{20}$$

Taking the derivative of V_2. With $|x|^\eta < 1 + |x|$ for $0 < \eta < 1$ in mind, one obtains

$$\begin{aligned} \dot{V}_2 &= s\dot{s} + \sigma_1 \dot{\sigma}_1 + \sigma_2 \dot{\sigma}_2 \\ &\le \frac{nB}{mJ}(1 + |\sigma_2|)|e_2 s| + k_1|\sigma_2 s| + k_2(1 + |s|)|\sigma_2| \\ &\quad + \frac{B}{J}|\sigma_2 e_2| + |\sigma_1 \sigma_2| + |\sigma_1 e_2| \\ &\le \frac{nB}{mJ}\frac{e_2^2 + s^2}{2} + \frac{nB}{mJ}\frac{\sigma_2^2 + s^2}{2}|e_2| + k_1\frac{\sigma_2^2 + s^2}{2} \\ &\quad + k_2\frac{\sigma_2^2 + 1}{2} + k_2\frac{\sigma_2^2 + s^2}{2} + \frac{B}{J}\frac{\sigma_2^2 + e_2^2}{2} \\ &\quad + \frac{\sigma_1^2 + \sigma_2^2}{2} + \frac{\sigma_1^2 + e_2^2}{2} \\ &\le K_v V_2 + L_v \end{aligned} \tag{21}$$

where $K_v = \max\left\{\frac{nB}{mJ}(1 + |e_2|) + k_1 + k_2, 2, \frac{nB}{mJ}|e_2| + k_1 + 2k_2 + \frac{B}{J} + 1\right\}$ and $L_v = \max\left\{\frac{nB}{2mJ}e_2^2 + \frac{k_2}{2} + \frac{B}{2J}e_2^2 + \frac{e_2^2}{2}\right\}$. Based on Theorem 1, it is evident that K_v and L_v are bounded positive constants. The system states will not escape to infinity before the finite-time convergence of observer error dynamics. Thus,

one has $z_2 = d$ for $t \geq t_f$. Choose the energy function V_3 as

$$V_3 = \frac{1}{2}s^2. \tag{22}$$

Taking the derivative of V_3, one obtains

$$\begin{aligned}\dot{V}_3 &= s\dot{s} \\ &= s\left[\lfloor\dot{\sigma}_1\rceil^{\alpha-1}(k_1 s + k_2\lfloor s\rceil^{\gamma})\right] \\ &\leq -\rho_1 V_3 - \rho_2 V_3^{\frac{\gamma+1}{2}}\end{aligned} \tag{23}$$

where $\rho_1 = 2\lfloor\dot{\sigma}_1\rceil^{n-1}k_1$ and $\rho_2 = 2^{\frac{\gamma+1}{2}}\lfloor\dot{\sigma}_1\rceil^{n-1}k_2$. According to the analysis in [32], σ_1 will not stay at zero, but switch around zero. Thus, it can prove that the system states reach the sliding mode surface $s = 0$ in finite time. After reaching the sliding mode surface, the dynamic is governed by

$$\dot{\sigma}_1 = -m\sigma_1^{\frac{1}{n}}. \tag{24}$$

From (24), one gets that the stability of the closed-loop PMSM system can be guaranteed under the u_s (6).

C. Step Three

According to the principle of the Karush–Kuhn–Tucker condition [33], when the current i_q reaches the upper constraint boundary, the control input is

$$u_q^* = R_s i_q + \omega_e i_d L_s + \omega_e \psi_m + L_s \tau_1 \overline{h}(i_q). \tag{25}$$

When the current i_q reaches the lower constraint boundary, the control input is

$$u_q^* = R_s i_q + \omega_e i_d L_s + \omega_e \psi_m - L_s \tau_1 \underline{h}(i_q). \tag{26}$$

First of all, we analyze the situation where the current is at the upper constraint boundary. Choose the energy function as

$$V_4 = \frac{1}{2}\sigma_1^2 + \frac{1}{2}i_q^2. \tag{27}$$

By combining (25) with (1) and taking the derivative of V_4, one obtains

$$\begin{aligned}\dot{V}_4 &= \sigma_1\dot{\sigma}_1 + i_q\dot{i}_q \\ &= \sigma_1\left(-\frac{K_t}{J}i_q - \frac{B}{J}\sigma_1 + \frac{B}{J}\omega_r + \frac{T_L}{J}\right) + i_q(-\tau_1 i_q + \tau_1 c) \\ &\leq -\frac{B}{J}\sigma_1^2 + \frac{(K_t i_q - B\omega_r - T_L)^2}{2BJ} + \frac{B}{2J}\sigma_1^2 \\ &\quad - \tau_1 i_q^2 + \frac{\tau_1 c^2}{2} + \frac{\tau_1 i_q^2}{2} \\ &= -K_{v2}V_4 + L_{v2}\end{aligned} \tag{28}$$

where $K_{v2} = \{\frac{B}{J}, \tau_1\}$ and $L_{v2} = \{\frac{(K_t i_q - B\omega_r - T_L)^2}{2BJ}, \frac{\tau_1 c^2}{2}\}$ are the positive constants. It can be concluded that when the current is at the upper constraint bound, the current i_q can converge to a bounded region. This means that i_q will not exceed the constraint boundary c, i.e., $i_q \leq c$ holds. Subsequently, the speed tracking error e_1 is also convergent. There are two situations. The first situation is when the condition $K_t c > B\omega_r + T_L$ holds, e_1 converges to a certain range, the current will leave the upper constraint boundary and $u_q^* = u_s$. Consequently, e_1 will converge to zero in finite time. The second situation occurs when $K_t c \leq B\omega_r + T_L$, the current i_q will remain on the constraint boundary. With (28) in mind, the speed will converge to a bounded region. Finally, in the case which i_q reaches the lower constraint boundary, the proof process is similar, so it is omitted. This completes the proof. ■

REFERENCES

[1] Y. Cui, Z. Yin, X. Cao, Y. Zhang, and Y. Liu, "Enhanced linear active disturbance rejection speed control of IPMSM based on interference differential compensation and cascaded linear extended state observer," *IEEE Trans. Power Electron.*, vol. 39, no. 10, pp. 13582–13596, Oct. 2024.

[2] Z. Zhou, S. Zhang, Z. Xu, Y. Peng, and X. Jin, "High-quality positioning strategy for biaxial contour machining system with nonlinear model predictive control," *IEEE Trans. Emerg. Sel. Topics Power Electron.*, vol. 11, no. 4, pp. 4355–4367, Aug. 2023.

[3] B. Dai, J. Sun, J. Yang, and S. Li, "Dynamic event-triggered disturbance rejection control for speed regulation of networked PMSM," *IEEE Trans. Ind. Inform.*, vol. 20, no. 4, pp. 6436–6445, Apr. 2024.

[4] M. Iwasaki, S. Kenta, and M. Yoshihiro, "High-precision motion control techniques: A promising approach to improving motion performance," *IEEE Ind. Electron. Mag.*, vol. 6, no. 1, pp. 32–40, Mar. 2012.

[5] P. Chen, Y. Luo, H. Gan, Y. Liu, and Y. Chen, "A current- and speed-loop decoupling controller for SPMSM under periodic disturbances," *IEEE Trans. Power Electron.*, vol. 39, no. 6, pp. 6889–6902, Jun. 2024.

[6] J. Mao et al., "Non-cascaded model-free predictive speed control of SMPMSM drive system," *IEEE Trans. Energy Convers.*, vol. 37, no. 1, pp. 153–162, Mar. 2022.

[7] J. Zhang, W. Ren, and X. Sun, "Current-constrained adaptive robust control for uncertain PMSM drive systems: Theory and experimentation," *IEEE Trans. Transport. Electrific.*, vol. 9, no. 3, pp. 4158–4169, Sep. 2023.

[8] J. Li, L. Zhang, L. Luo, and S. Li, "Extended state observer based current-constrained controller for a PMSM system in presence of disturbances: Design, analysis and experiments," *Control Eng. Pract.*, vol. 132, 2023, Art. no. 105412.

[9] J. Zhang, W. Ren, J. Li, and X. Sun, "Adaptive neural asymptotic tracking control for PMSM systems under current constraints and unknown dynamics," *IEEE Trans. Circuits Syst., II, Exp. Briefs*, vol. 71, no. 2, pp. 777–781, Feb. 2024.

[10] Y. Tan, J. Yang, J. Liu, and S. Li, "Design of current-risk-aware disturbance rejection controller for speed regulation of PMSMs," *Control Eng. Pract.*, vol. 146, 2024, Art. no. 105875.

[11] B. Dai and Z. Wang, "Disturbance observer-based sliding mode control using barrier function for output speed fluctuation constraints of PMSM," *IEEE Trans. Energy Convers.*, vol. 39, no. 2, pp. 1192–1201, Jun. 2024.

[12] X. Liu and H. Yu, "Continuous adaptive integral-type sliding mode control based on disturbance observer for PMSM drives," *Nonlinear Dyn.*, vol. 104, no. 2, pp. 1429–1441, 2021.

[13] J. Yang, Y. Li, and S. Tong, "Adaptive NN finite-time tracking control for PMSM with full state constraints," *Neurocomputing*, vol. 443, pp. 213–221, 2021.

[14] J. Wang and Y. Wang, "Nonlinear filtering-based output tracking error constraint control for permanent magnet synchronous motors with complete unknown coefficients," *Int. J. Adapt. Control Signal Process*, vol. 37, no. 1, pp. 264–277, 2023.

[15] Y. Xu, S. Li, W. Zhang, G. Yu, and J. Zou, "Long-horizon constrained model predictive direct speed control for PMSM drives based on Laguerre functions," *IEEE Trans. Control Syst. Technol.*, vol. 32, no. 3, pp. 1002–1014, May 2024.

[16] J. Yang, W. Zheng, S. Li, B. Wu, and M. Cheng, "Design of a prediction-accuracy-enhanced continuous-time MPC for disturbed systems via a disturbance observer," *IEEE Trans. Ind. Electron.*, vol. 62, no. 9, pp. 5807–5816, Sep. 2015.

[17] T. Guo, Z. Sun, X. Wang, S. Li, and K. Zhang, "A simple current-constrained controller for permanent-magnet synchronous motor," *IEEE Trans. Ind. Inform.*, vol. 15, no. 3, pp. 1486–1495, Mar. 2019.

[18] C. Dai, T. Guo, J. Yang, and S. Li, "A disturbance observer-based current-constrained controller for speed regulation of PMSM systems subject to unmatched disturbances," *IEEE Trans. Ind. Electron.*, vol. 68, no. 1, pp. 767–775, Jan. 2021.

[19] A. Ames, X. Xu, J. Grizzle, and P. Tabuada, "Control barrier function based quadratic programs for safety critical systems," *IEEE Trans. Autom. Control*, vol. 62, no. 8, pp. 3861–3876, Aug. 2017.
[20] Y. Wang and X. Xu, "Disturbance observer-based robust control barrier function," in *Proc. Amer. Control Conf.*, 2022, pp. 3681–3687.
[21] B. Li, S. Wen, Z. Yan, G. Wen, and T. Huang, "A survey on the control Lyapunov function and control barrier function for nonlinear-affine control systems," *IEEE/CAA J. Automatica Sinica*, vol. 10, no. 3, pp. 584–602, Mar. 2023.
[22] J. Sun, J. Yang, and Z. Zeng, "Safety-critical control with control barrier function based on disturbance observer," *IEEE Trans. Autom. Control*, vol. 69, no. 7, pp. 4750–4756, Jul. 2024.
[23] Y. Yan, J. Yang, Z. Sun, C. Zhang, S. Li, and H. Yu, "Robust speed regulation for PMSM servo system with multiple sources of disturbances via an augmented disturbance observer," *IEEE/ASME Trans. Mechatron.*, vol. 23, no. 2, pp. 769–780, Apr. 2018.
[24] S. You, S. Lee, S. Lim, S. Kim, and C. Ahn, "Model-free filter for servo drive applications via error dynamics diagonalization technique," *IEEE Trans. Circuits Syst. I, Reg. Papers*, vol. 71, no. 4, pp. 1901–1909, Apr. 2024.
[25] Z. Zhang and X. Liu, "An improved super-twisting sliding mode single loop control with current-constraint for PMSM based on two-time scale disturbance observer," *IEEE Trans. Transport. Electrific.*, vol. 10, no. 3, pp. 5389–5399, Sep. 2024.
[26] M. Tian, T. Wang, Y. Yu, Q. Dong, B. Wang, and D. Xu, "Integrated observer-based terminal sliding-mode speed controller for PMSM drives considering multisource disturbances," *IEEE Trans. Power Electron.*, vol. 39, no. 7, pp. 7968–7979, Jul. 2024.
[27] L. Chen, H. Zhang, H. Wang, K. Shao, G. Wang, and A. Yazdani, "Continuous adaptive fast terminal sliding mode-based speed regulation control of PMSM drive via improved super-twisting observer," *IEEE Trans. Ind. Electron.*, vol. 71, no. 5, pp. 5105–5115, May 2024.
[28] J. Yang, S. Li, J. Su, and X. Yu, "Continuous nonsingular terminal sliding mode control for systems with mismatched disturbances," *Automatica*, vol. 49, no. 7, pp. 2287–2291, 2013.
[29] K. Zuo, F. Wang, Z. Li, D. Ke, R. Kennel, and M. Heldwein, "A robust unified strategy for maximum torque per ampere and field weakening in permanent magnet synchronous motor," *IEEE Trans. Power Electron.*, vol. 39, no. 5, pp. 5286–5297, May 2024.
[30] Z. Liu, K. Mao, X. Lei, S. Zheng, and H. Zhang, "Loss minimization control based on bivariate extreme value theory for PMSMs," *IEEE Trans. Power Electron.*, vol. 39, no. 2, pp. 2004–2012, Feb. 2024.
[31] L. Zhao, S. Gu, J. Zhang, and S. Li, "Finite-time trajectory tracking control for rodless pneumatic cylinder systems with disturbances," *IEEE Trans. Ind. Electron.*, vol. 69, no. 4, pp. 4137–4147, Apr. 2022.
[32] Y. Feng, X. Yu, and Z. Man, "Non-singular terminal sliding mode control of rigid manipulators," *Automatica*, vol. 38, no. 12, pp. 2159–2167, 2002.
[33] S. Boyd, S. P. Boyd, and L. Vandenberghe, *Convex Optimization*. Cambridge, U.K.: Cambridge Univ. Press, 2004.
[34] C. He, J. Hu, and Y. Li, "Predictive position control with system constraints for PMSM drives based on geometric optimization," *IEEE Trans. Ind. Electron.*, vol. 70, no. 8, pp. 7773–7782, Aug. 2023.

Bin Dai received the B.S. and M.S. degrees both in electrical engineering from Nantong university, Nantong, China, in 2016 and 2019, and the Ph.D degree in advanced manufacturing from the School of Automation, Southeast University, Nanjing, China in 2024.

He is currently a Lecturer with the College of Information Science and Technology & Artificial Intelligence, Nanjing Forestry University, Nanjing, China. His research interests include disturbance rejection control, safety-critical control, and nonlinear control theory with applications to mechatronic systems.

Zuo Wang (Member, IEEE) received the B.Eng. degree in automation from Hohai University, Nanjing, China, in 2013, and the Ph.D. degree in automatic control from Southeast University, Nanjing, China, in 2020.

Since 2020, he has been with the School of Automation, Southeast University. His research interests include advanced control theory and its application to power electronics, ac motor control systems, and spacecraft attitude systems.

Jianfeng Zhao received the B.S. degree from Huainan Mining Institute, Anhui, China, in 1995, the M.S. degree from the Nanjing University of Aero nautics and Astronautics, Nanjing, China, in 1998, and the Ph.D. degree from the Southeast University, Nanjing, China, in 2001.

He joined the Faculty of the School of Electrical Engineering, Southeast University, where he has been a Professor, since 2008, and the Dean, from 2014 to 2022. He is currently the Vice President of the Nanjing Forestry University, Nanjing, China. He has authored more than 150 technical papers and holds 60 Chinese patents and two U.S. patents. His research interests include utility applications of power electronics in smart grids, such as solid-state transformers, active filters for power conditioning, flexible ac transmission system devices, multilevel ac motor drivers, and efficient energy utilization.

Shihua Li (Fellow, IEEE) received the bachelor's, master's, and Ph.D. degrees in automatic control from Southeast University, Nanjing, China, in 1995, 1998 and 2001, respectively.

Since 2001, he has been with School of Automation, Southeast University, where he is currently a Professor and the Director of Mechatronic Systems Control Laboratory. His research interests include modeling, analysis and nonlinear control theory with applications to mechatronic systems, including manipulator, robot, ac motor, power electronic systems, and others.